Research Article

Journal of Plasma Chemistry and Plasma Processing Research

Application of The Classical Soliton Theory to Study the Dynamics in Passive-Dispersed and Active-Relaxation Media During the Formation of a Twist in A Toroidal Plasma

Sergey Belyakin[1*], Alexander Stepanov[2]

[1]*Department of General Physics, Physics Faculty, Lomonosov Moscow State University, Moscow, Russia*

[2]*Department of Oscillation Physics, Physics Faculty, Lomonosov Moscow State University, Moscow, Russia*

[*]Corresponding author
Sergey Belyakin, Department of General Physics, Physics Faculty, Lomonosov Moscow State University, Moscow, Russia

Submitted: 13 Jul 2022; **Accepted:** 18 Jul 2022; **Published:** 25 Jul 2022

Citation: *Sergey Belyakin, Alexander Stepanov. (2022). Application of the classical soliton theory to study the dynamics in passive-dispersed and active-relaxation media during the formation of a twist in a toroidal plasma. J Pla Che Pla Pro Res, 3 (1): 26-36.*

Abstract

In this paper we consider the possibility of using analog models to study the behavior of the evolution and dynamics of toroidal vortex flows. The current model based on coupled van der Pol generators is used as the main one. In this robot, based on nonlinear dynamics display Bernoulli presented the evolution of the Torus. The use of analog models makes it possible to trace the dynamics of vortex flows. In General, the presented results allow us to confidently assert that both in the experiment and in the theoretical consideration we are dealing with the same object - a strange attractor of the Smale – Williams type in a non-Autonomous oscillatory system. The available data suggest that it is an attractor of hyperbolic type, although, strictly speaking, this statement needs mathematical proof. The appearance of an example of a physical system with a hyperbolic chaotic attractor is of fundamental importance for the further development of nonlinear dynamics and its applications. This is, in a sense, a "breakthrough into the hyperbolic realm." Based on the inherent property of coarseness of hyperbolic attractors, we can build other examples of systems with hyperbolic chaos. The presence of such physical systems opens up opportunities for the application of a deeply studied branch of mathematics – hyperbolic theory, and also translates into practice the problem of comparative study of hyperbolic and non-hyperbolic chaos in theory and experiment. This system can be used to study toroidal vortex processes.

Keywords: Nonlinear Dynamic System, Toroidal Vortices, Display Bernoulli, Analog Models

Introduction

The conditions for the formation of a swirl in a toroidal vortex of a stellarator Fig.1.

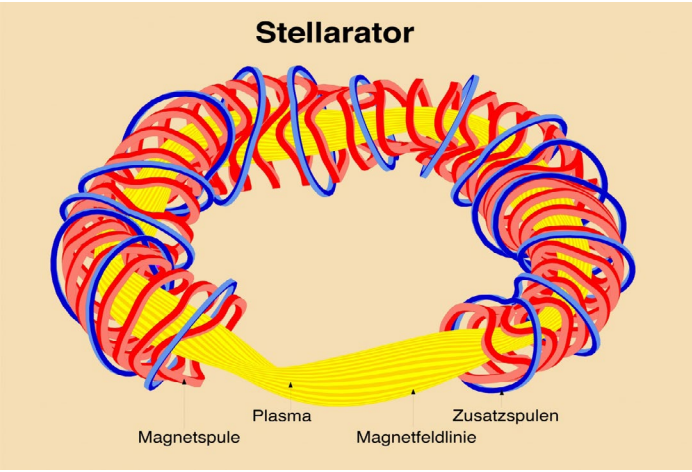

Figure 1: The conditions for the formation of a swirl in a toroidal vortex of a stellarator

A toroidal vortex in a stable dynamic state is presented. In the third part Fig.2. the bifurcation of a toroidal vortex is presented. Geometric constructions of hyperbolic attractors the Smale-Williams Attractor [1-3] is presented in Fig.2.

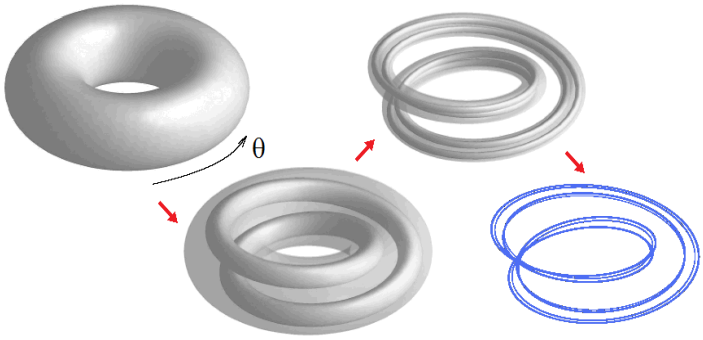

Figure 2: Evolution of a strange attractor of hyperbolic type. Bifurcation of a toroidal vortex

The mathematical theory of chaos, based on a strict axiomatic

Foundation, deals with strange attractors of the hyperbolic type Fig.2. In such an attractor, all orbits belonging to it in the phase space of the system are saddle, and stable and unstable manifolds (invariant sets composed of trajectories approaching the original one in forward or reverse time) intersect transversally, i.e. without touching.

Hyperbolic strange attractors are robust (structurally stable). This means the insensitivity of the nature of the movements and the relative position of the trajectories in phase space with respect to the variation of the equations of the system. In contrast to the hyperbolic attractor, quasi-attractors are characterized by a sensitive dependence of dynamics details on parameters. It is clearly desirable for potential applications of chaos such as communication, masking of signals, etc. Thus, from a fundamental and applied point of view it is interesting to realize hyperbolic chaos in physical systems.

In textbooks and monographs on nonlinear dynamics, examples of hyperbolic attractors are represented by abstract constructions. For example, the Smale-Williams attractor is constructed to map three-dimensional space into itself, defined by the following procedure. Consider a region in the form of a torus, stretch it in length, fold it in half and enclose it in the original torus, as shown in the figure. At each next iteration the number of" turns " doubles. An object that is obtained within the limit of a large number of iterations is called a Smale – Williams solenoid. Its transverse structure has the form of a Cantor set [4 -7].

If we introduce the angular coordinate of the image point *q*, then on successive iterations it obviously obeys the Bernoulli map $q_{n+1}=\{2q_n\}$. In the remaining two directions, the phase volume element undergoes compression. Therefore, a system of coupled non-Autonomous generators appears to be a suitable candidate for the implementation of the Smale - Williams attractor.

Consider the one-dimensional map: $x_{n+1}=\{2x_n\}$, where the braces denote the fractional part of the number. Its graph and diagram, illustrating the dynamics over several iterations, is shown in Fig.3.

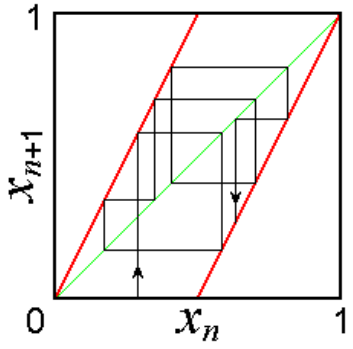

Figure 3: A one-dimensional map $x_{n+1}=\{2x_n\}$, where braces denote the fractional part of the number, the graph and chart illustrate the dynamics over several iterations.

It is convenient to represent the variable x in the binary notation, with the digit 0 in the first position after the dividing point corresponds to the location of the representing point in the left, and 1 - in the right half of the unit interval. Suppose, for example, one step of evolution in time is that the sequence of zeros and ones is shifted to the left by one position, and the figure that is on the left side of the dividing point is discarded, and so on. This transformation of the binary sequence, consisting in the shift of all characters by one position, called Bernoulli shift.

We define the initial state of the random sequence of digits, for example, obtained by flipping coins, according to the rule of the *eagle* is 0, *tails* are 1: $x_0 = 0.0101101...$ Then, in iterations, the image point will visit the left or right half of the unit interval exactly following our random sequence, thus creating chaos. It is clear that the small perturbation of the initial condition is doubled in one iteration step. Therefore, the *Lyapunov exponent* for this map is ln 2 = 0.693.

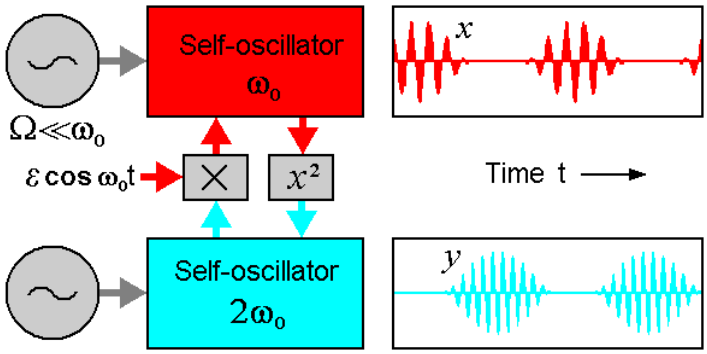

Figure 4: Non-Autonomous oscillatory system based on two oscillators with characteristic frequencies ω_0 and $2\omega_0$.

How to implement the dynamics corresponding to the Bernoulli map in a physical system. Let us turn to the one shown in Fig.4 flowchart. It is a non-Autonomous oscillatory system based on two oscillators with characteristic frequencies ω_0 and $2\omega_0$. The parameter controlling the excitation of one and the other oscillator slowly changes in time in antiphase with period T, which is an integer number of periods of the fundamental frequency: $T = 2\pi N/\omega_0$. Thus, alternately excited one, then the other generator. The effect of the first generator on the second is produced through a nonlinear quadratic element. The generated second harmonic serves as a seed when the second generator is excited. In turn, the second generator acts on the first through a nonlinear element that mixes the incoming signal and the auxiliary reference signal at a frequency ω0. In this case, a component appears at the difference frequency. It resonates with the first generator and serves as a seed when it begins to generate. Both generators, as it were, in turn transmit excitation to one another.

Let us explain why the scheme functions as a chaos generator. Suppose that at the generation stage of the first oscillator the oscillations have some phase φ. The signal at the output of the coupling element contains a second harmonic, and its phase 2φ is transmit-

ted to the second oscillator when it begins to generate. By mixing with the reference signal on the second coupling element, the doubled phase is transferred to the original frequency range, so that when the first oscillator is excited, at the next generation stage, it will receive a phase of 2φ. At successive stages of excitation of the first generator for its phase normalized to 2π, Θ = φ/2π, the Bernoulli map will be valid: $\Theta_{n+1} = \{2\Theta_n\}$. To observe the described mechanism numerically, we consider a system of equations (1), two van Der Pol oscillators with variable coefficients (1):

$$\ddot{x} - (A\cos 2\pi t/T - x^2)\dot{x} + \omega_0^2 x = \varepsilon y \cos\omega_0 t,$$
$$\ddot{y} - (-A\cos 2\pi t/T - y^2)\dot{y} + \omega_0^2 y = \varepsilon x^2 .$$

For fig.5 shows the time dependence of the variables x and y in this system, which performs chaotic motion during relay transmission of excitation from one oscillator to another. The graph is based on the results of the numerical solution of the equations for $\omega_0 = 2\pi$, T = 10, A = 3, ε = 0.5.

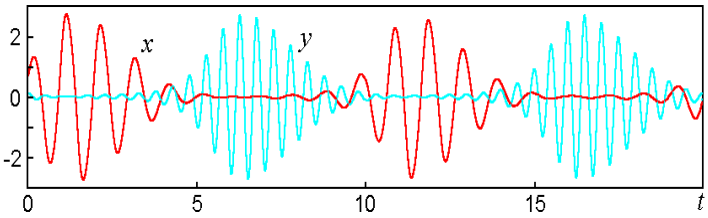

Figure 5: The time dependence of the variables x and y in this system, which performs chaotic motion during relay excitation transfer from one oscillator to another at ω0 = 2π, T = 10, A = 3, ε = 0.5, is shown.

For fig.6 shows the time dependence of the variables x and y in this system, making a chaotic motion in the relay transmission of excitation from one oscillator to another. The graph is based on the results of the numerical solution of the equations for $\omega_0 = 2\pi$, T = 6, A = 5, ε = 0.5.

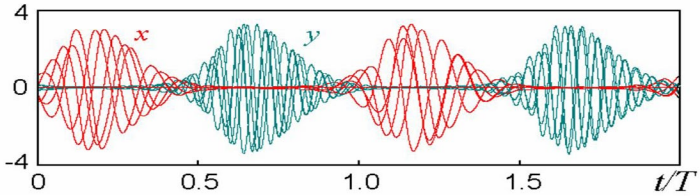

Figure 6: The time dependence of the variables x and y in this system, which performs chaotic motion during relay transfer of excitation from one oscillator to another at $\omega_0 = 2\pi$, T = 6, A = 5, ε = 0.5, is shown.

Chaos manifests itself in a random walk of the maxima and minima of the filling relative to the envelope. Below is an empirical mapping diagram for the phase of the first oscillator in the middle of the excitation stages. Fig.7 shows the points (Θ_n, Θ_{n+1}) for a sufficiently large number of t periods.

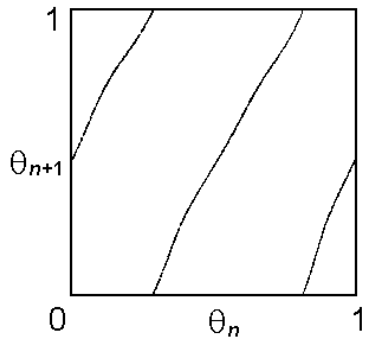

Figure 7: Points (Θ_n, Θ_{n+1}) are postponed at sufficiently large number of periods *T*.

So, we obtain a map which, despite having some deformations, is topologically equivalent to the Bernoulli map $\Theta_{n+1} = \{2\Theta_n\}$. In fact, if we vary the initial phase so that the image points once bypassed the full circle, the point-image will make a two-fold circumnavigation of the circle. This is expressed in the fact that the graph has two branches located in the same way as in the first figure at the beginning of this page. The correspondence with the classical Bernoulli map becomes better with increasing the period ratio of *N*.

For fig.8 a graph of the dependence of the higher Lyapunov exponent (Λ) for a system of coupled non-Autonomous van der Pol oscillators on the amplitude of the slow modulation A at fixed other parameters is presented, and the T period t is taken as a unit of time.

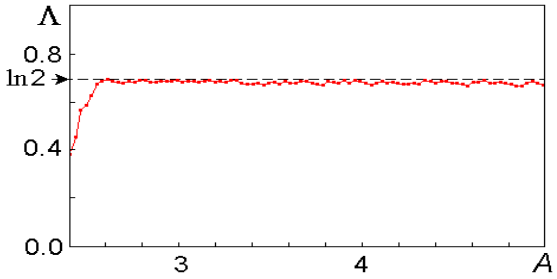

Figure 8: A graph of the dependence of the higher Lyapunov exponent (Λ), for a system of coupled non-Autonomous van der Pol oscillators on the amplitude of the slow modulation A at fixed other parameters is presented.

As you can see, in a wide range of the parameter, the Lyapunov exponent remains almost constant and is approximately equal to ln2 = 0.693, which corresponds to the Bernoulli map. At small A the correspondence disappears - the Lyapunov exponent becomes noticeably smaller.

Current Model Based on Coupled van Der Pol generators

Let us turn to the scheme of the radio engineering device shown in fig.9 [2,8].

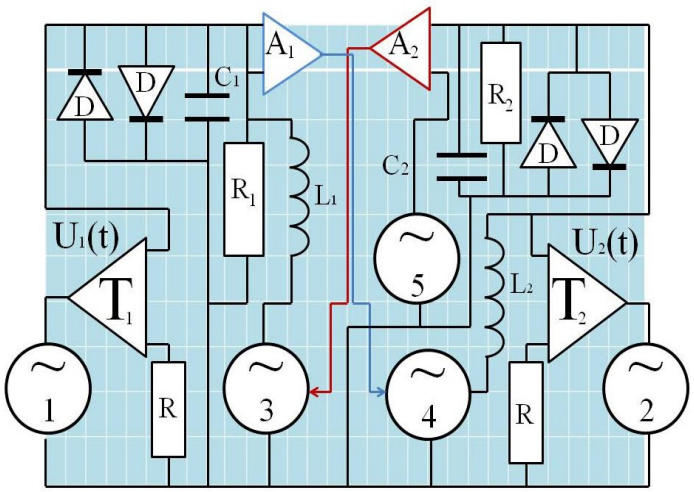

Figure 9: The scheme of the radio engineering device, which is a non-Autonomous oscillatory system assembled on the basis of two subsystems of van Der Pol oscillators with periodically changing parameters.

Each of the two subsystems - generators contains an oscillatory circuit formed by an inductor $L_{1,2}$ and a capacitance $C_{1,2}$, and the natural frequency of the second is twice as large as the first. The negative resistance - $R_{1,2}$ is introduced by the element based on the operational amplifier. The increase in energy losses with increasing vibration amplitude is provided by a nonlinear element composed of semiconductor diodes (D). The field-effect transistor introduces a positive conductivity, the value of which is regulated by the voltage supplied to the gate. It slowly changes in time with a period T in the opposite phase for the first and second generator, which ensures their alternate excitation. The first generator acts on the second through a nonlinear quadratic element A1, generating a second harmonic, and the second on the first through a nonlinear element A2, mixing the second harmonic and the auxiliary signal at a frequency $\omega_0 = 1/\sqrt{(L_1C_1)}$ and $2\omega_0 = 1/\sqrt{(L_2C_2)}$.

We present the dynamics of the proposed scheme for each subsystem and write the Kirchhoff equation (2), expressing the equality of zero total current in the parallel branches of the scheme equation, linking the voltage and current through the inductor:

$$\dot{u} = -x\omega^2 + \left(-x^2 + A_1 \cos\frac{2\pi t}{N}\right)u + \varepsilon_1 y \cos\omega t,$$

$$\dot{x} = u,$$

$$\dot{y} = -y\omega^2 + \left(-y^2 - A_2 \cos\frac{2\pi t}{N}\right)v + \varepsilon_2 x^2,$$

$$\dot{y} = v.$$

$$\dot{z} = xy \sinh x \sinh y \sin\omega_0 t \cos\omega_0 t.$$

In equation (2), the function $f(U) \approx \alpha U + \beta U3$ characterizes the current – voltage dependence for a nonlinear element composed of semiconductor diodes (D), k1,2 - the transmission coefficients in the circuits providing the connection between the two subsystems. The factor $q \pm ka \cos(\omega 0t/N)$ corresponds to the conductivity introduced into the circuit by a field-effect transistor in the presence of an alternating gate voltage $\pm a \cos(\omega 0t/N)$. After replacement of variables providing reduction to the dimensionless form, receive:

$$X = \frac{2x}{1+x^2+y^2}, Y = \frac{2y}{1+x^2+y^2}$$

In equation (3) dimensionless variables x and u characterize the voltage and current in the oscillating circuit of the first generator (respectively, U_1 and I_1), and y and v - voltage and current in the second oscillating circuit (U_2 and I_2). Time is normalized for the period of natural oscillations of the primary circuit. Parameters A_1 and A_2 determine the amplitude of the slow modulation of the parameter responsible for the Andronov - Hopf bifurcation in the first and second oscillator, and h_1 and h_2 determine the offset of the mean value of this parameter relative to the bifurcation point. Finally, ε1 and ε2 are the communication parameters between subsystems.

The system described (Fig.9) was implemented as a laboratory device, with the natural frequencies of the oscillating circuits being approximately 1090 and 2180 Hz. Voltages U_1 and U_2, respectively, removed from the first and second circuits, could be fed to the recording equipment (oscilloscope, spectrum analyzer) or entered into the computer in the form of a time series through an analog-to-digital Converter. The time derivative was obtained as a result of analog differentiation using a standard differentiation chain containing a capacitance, resistor, and operational amplifier.

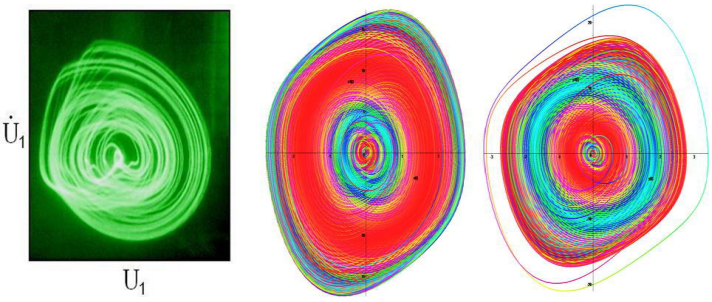

Figure 10: On the left is a photo from the oscilloscope screen of the attractor portrait projected onto the plane of the dynamic variables of the first oscillator (U1,U̇1). To the right is the phase portrait of ($x_{n+1} - x_n$, $x_{n+1} + x_n$) when the value of the parameters N = 10, $A_1 = A_2 = 3$, $\varepsilon_1 = \varepsilon_2 = 0.5$, $\omega_0 = 2\pi$.

Pair in Fig.10 shows portraits of the attractor projected onto a plane where the generalized coordinate (stress) and velocity (time derivative of stress) for the oscillator are plotted along the coordinate axes at N = 8. A color portrait of the attractor was photographed directly from the oscilloscope screen. The second portrait is obtained from solving equations on a computer. It is represented in red tones, where the brightness of the image is proportional to the relative residence time at the corresponding points.

In the experiment, with proper selection of parameters, chaotic oscillations were observed in the system due to relay transmission of excitation from one oscillator to another. For fig.11 typical samples of time dependences of voltage in the mode of regular generation of hyperbolic chaos in this subsystem are shown at the ratio of frequency of slow change of parameters at N = 10 and Fig.12 frequencies of the auxiliary signal N = 6 of multiple bifurcation, - in experiment and by results of the numerical solution of system of the equations. The experimental graph is built on a computer using time series recorded in memory, obtained by analog-to-digital conversion of voltages $U_1(t)$ and $U_2(t)$.

For fig.13 shows typical samples of the time dependences of the voltage in the chaotic generation mode in this subsystem with a ratio of the frequency of a slow change in parameters at N = 8 signal frequencies with equal amplitudes $A_1 = 0.8$, $A_2 = 0.2$, and a complex regular pattern of chaos was observed in this subsystem.

For fig.14 typical samples of time dependences of voltage in the mode of chaotic generation in this subsystem are shown at the ratio of frequency of slow change of parameters at signal frequencies N=8 with equal amplitudes $A_1 = 1.5$, $A_2 = 6.0$, a complex irregular pattern of hyperbolic chaos generation in this subsystem was observed.

For fig.15 typical samples of time dependences of voltage in the mode of chaotic generation in this subsystem are shown at the ratio of frequency of slow change of parameters at signal frequencies N=4 with equal amplitudes $A_1 = 1.5$, $A_2 = 6.0$, a complex irregular pattern of hyperbolic chaos generation in this subsystem was observed.

For fig.16 typical samples of time dependences of voltage in the mode of chaotic generation in this subsystem are shown at the ratio of frequency of slow change of parameters at signal frequencies N=8 with equal amplitudes $A_1 = 0.8$, $A_2 = 0.2$, a complex regular pattern of chaos generation in this subsystem was observed.

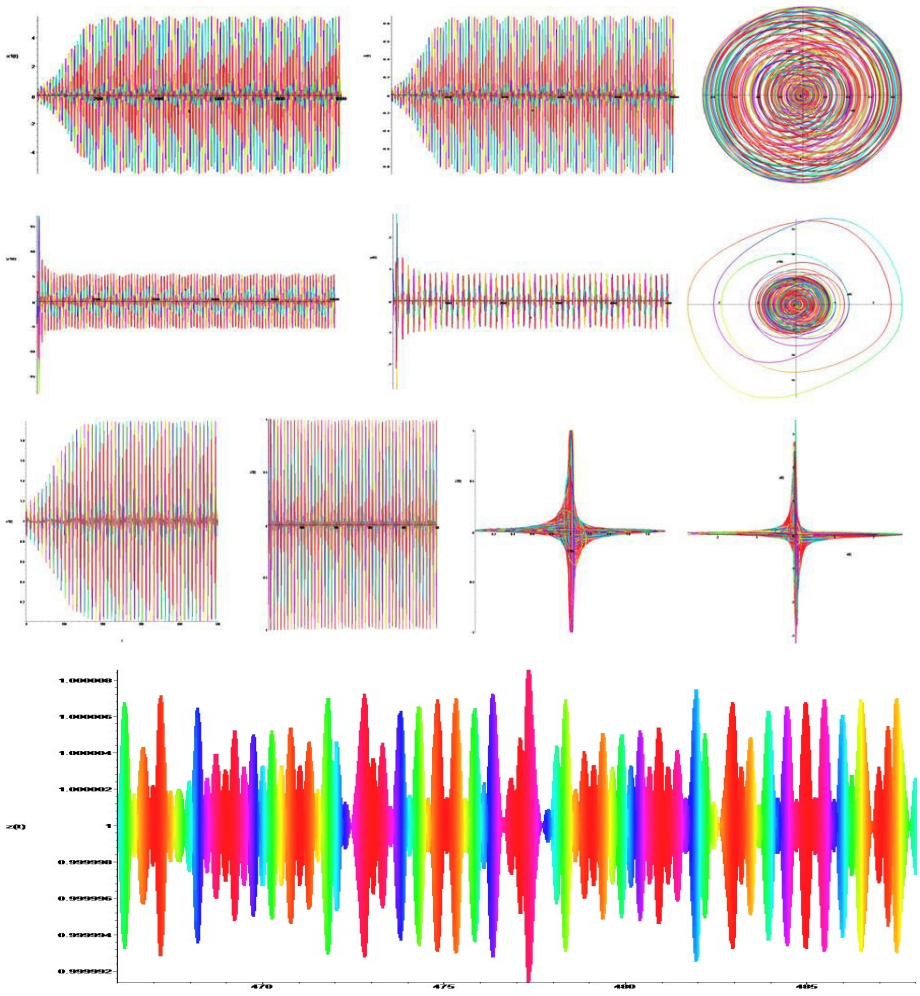

Figure 11: The upper figure shows the time dependences y(t) and v(t) on the left, the phase dependences $(y,\dot{y})$ and $(v,)$ on the right. The lower figure shows: left to right time dependencies x(t) and $x^2(t)$, at the bottom (x_n,x_{n+1}) and Fourier spectrum. At the value N = 10, $A_1 = 3.0$, $A_2 = 3.0$, $\varepsilon_1 = \varepsilon_2 = 0.5$, $\omega_0 = 2\pi$.

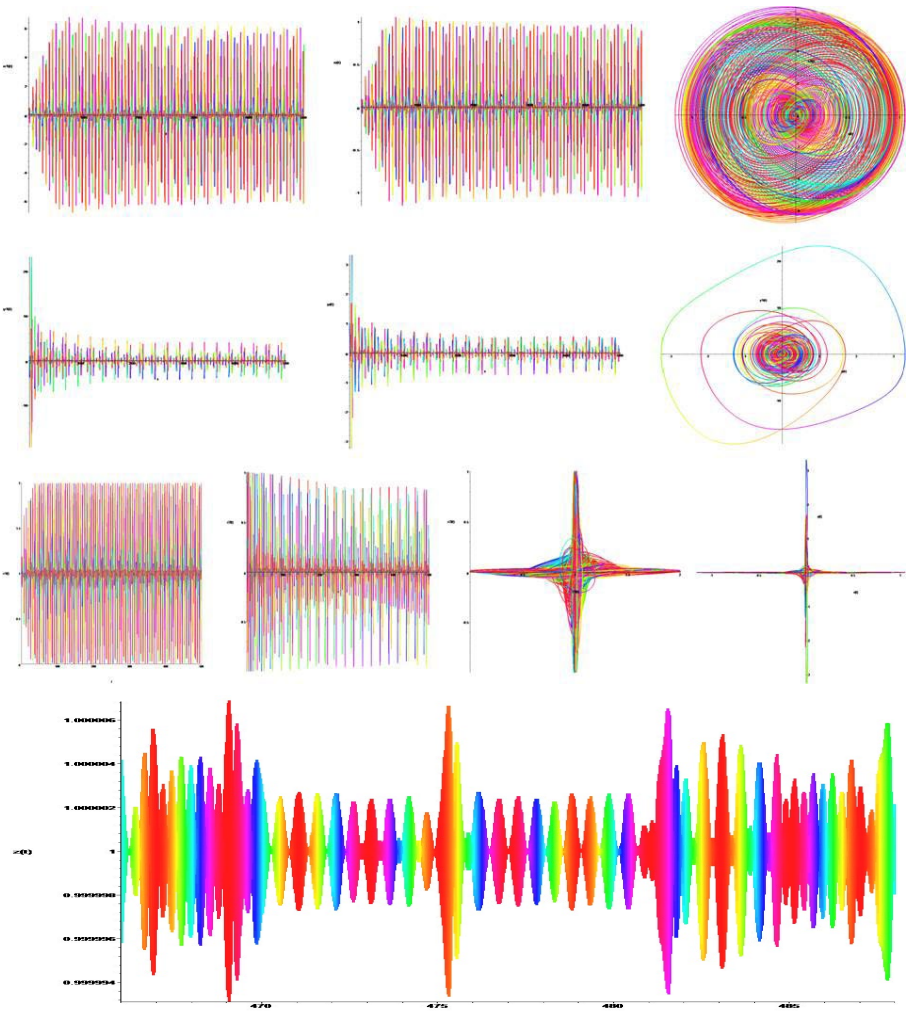

Figure 12: The upper figure shows the time dependences y(t) and v(t) on the left, the phase dependences (y,ẏ) and (v,) on the right. The lower figure shows: left to right time dependencies x(t), x^2 (t) and (x_n,x_{n+1}), at the bottom (x_n - x_{n+1}, x_n + x_{n+1}) and Fourier spectrum. At the value N = 6, A_1 = 5.0, A_2 = 5.0, $\varepsilon_1 = \varepsilon_2$ = 0.5, $\omega_0 = 2\pi$.

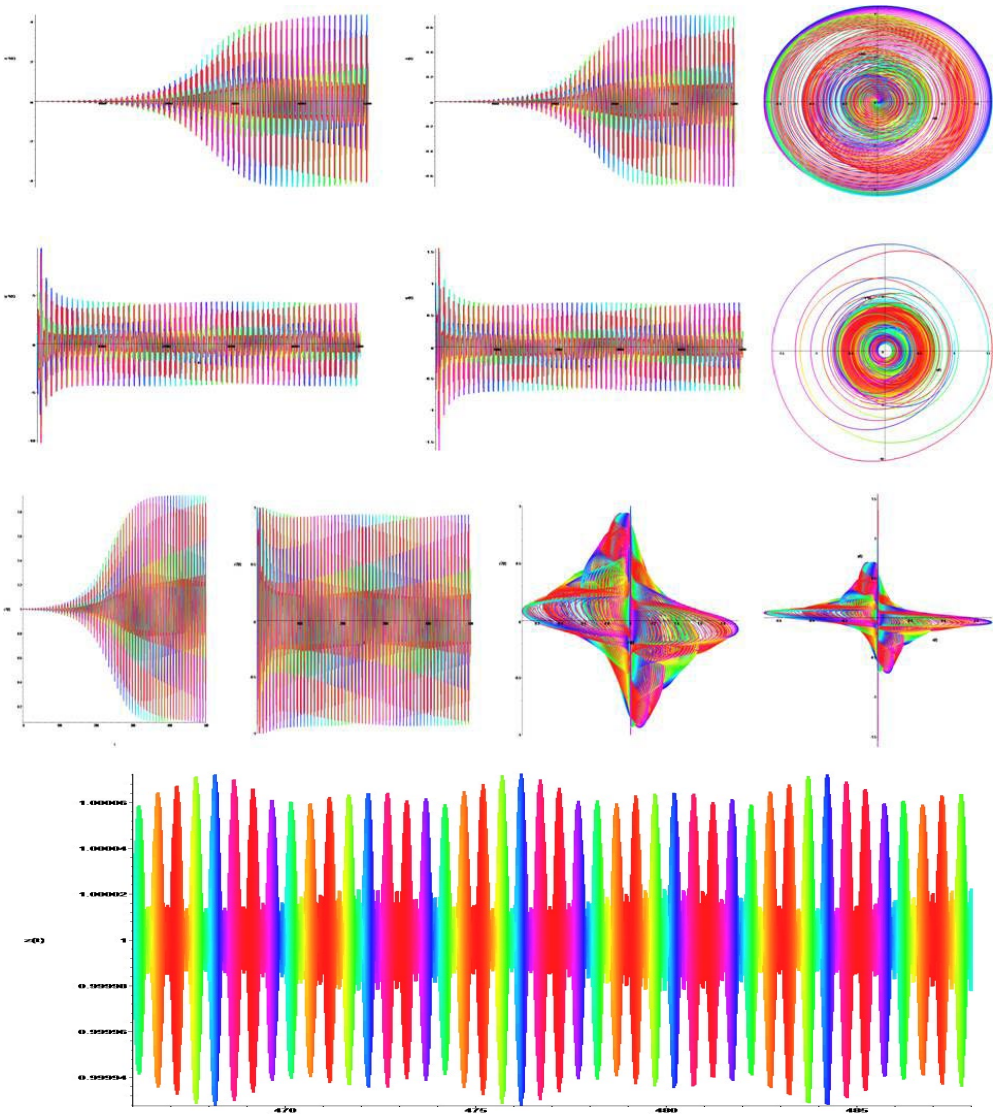

Figure 13: The upper figure shows the time dependences y(t) and v(t) on the left, the phase dependences (y,ẏ) and (v,) on the right. The lower figure shows: left to right time dependencies x(t), x2(t) and (xn,xn+1), at the bottom (x_n - x_{n+1}, x_n + x_{n+1}) and Fourier spectrum. At the value N = 8, A_1 = 0.8, A_2 = 0.2, $\varepsilon_1 = \varepsilon_2$ = 0.5, $\omega_0 = 2\pi$.

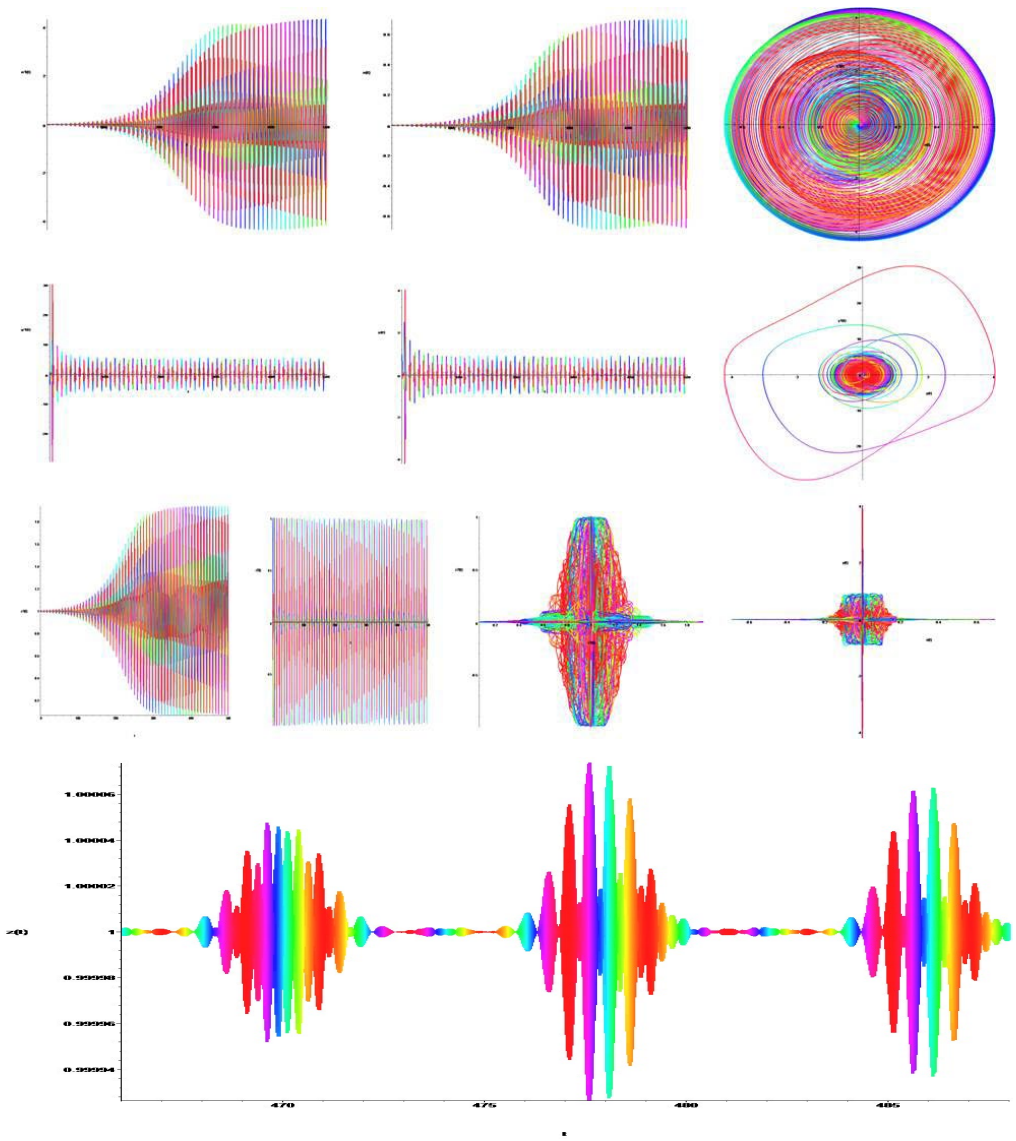

Figure 14: The upper figure shows the time dependences y(t) and v(t) on the left, the phase dependences (y,ẏ) and (v) on the right. The lower figure shows: left to right time dependencies x(t), x^2 (t) and (x_n, x_{n+1}), at the bottom (x_n - x_{n+1}, x_n + x_{n+1}) and Fourier spectrum. At the value N = 8, A_1 =1.5, A_2 = 6.0, $\varepsilon_1 = \varepsilon_2 = 0.5$, $\omega_0 = 2\pi$.

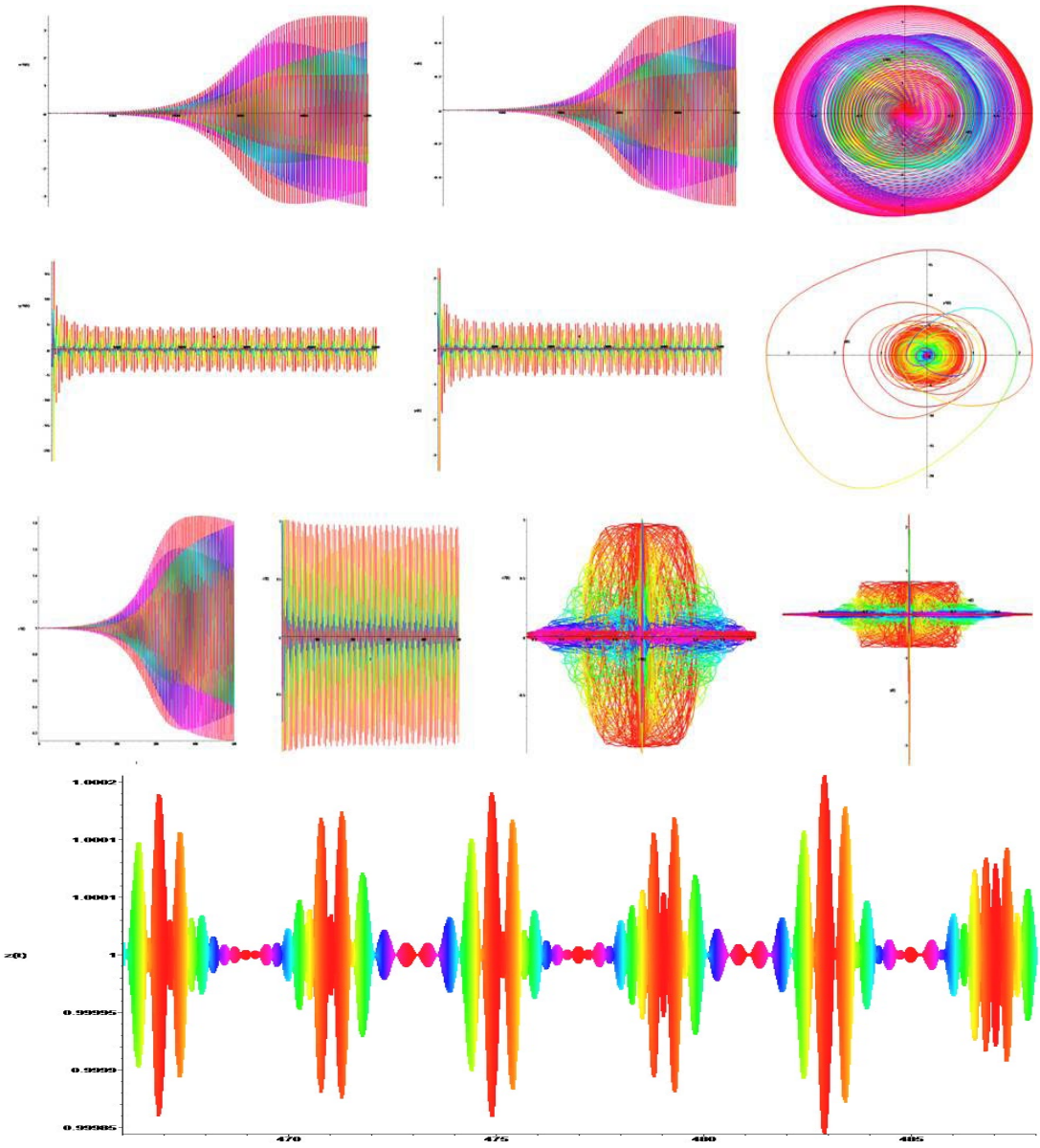

Figure 15: The upper figure shows the time dependences y(t) and v(t) on the left, the phase dependences (y,ẏ) and (v) on the right. The lower figure shows: left to right time dependencies x(t), x^2 (t) and (x_n, x_{n+1}), at the bottom (x_n - x_{n+1}, x_n + x_{n+1}) and Fourier spectrum. At the value N = 4, A_1 =1.5, A_2 = 6.0, $\varepsilon_1 = \varepsilon_2 = 0.5$, $\omega_0 = 2\pi$.

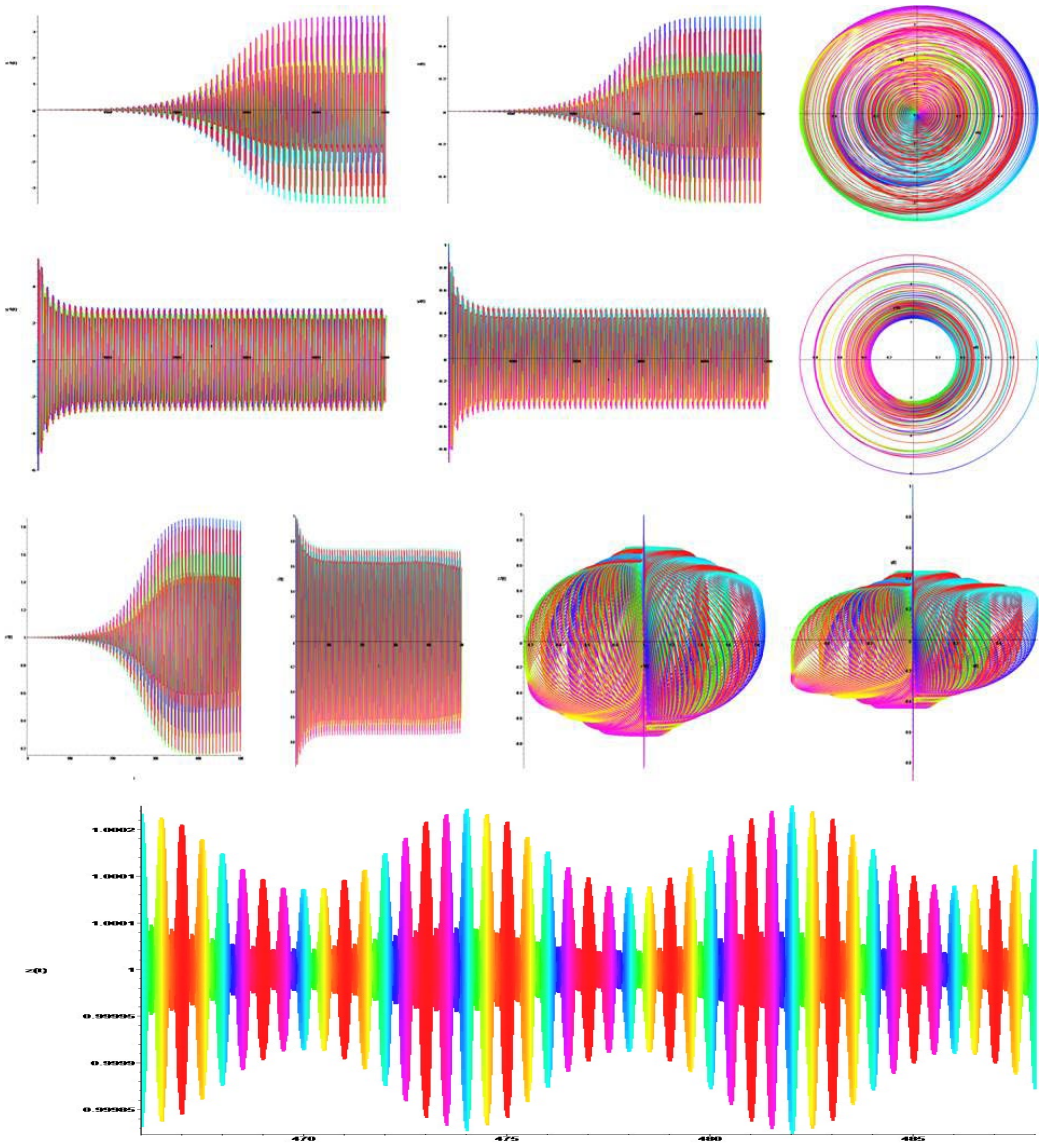

Figure 16: The upper figure shows the time dependences y(t) and v(t) on the left, the phase dependences (y,ẏ) and (v) on the right. The lower figure shows: left to right time dependencies x(t), x^2 (t) and (x_n, x_{n+1}), at the bottom (x_n - x_{n+1}, x_n + x_{n+1}) and Fourier spectrum. At the value N = 8, A_1 =0.8, A^2 = 0.2, $\varepsilon_1 = \varepsilon_2$ = 0.5, $\omega_0 = 2\pi$.

Conclusion

This paper presents a dynamic classical soliton model for studying the conditions for the formation of a swirl in a toroidal vortex of a stellarator. It is represented by a geometric construction of the evolution of the Smale-Williams hyperbolic attractor. Two coupled Van der Pol generators are used as the main model qn+1={2qn}. The Bernoulli map, based on non-linear dynamics, is an evolution of the torus. The use of a dynamic classical soliton model makes it possible to find the conditions for the formation of a swirl in a toroidal vortex, which can be determined visually using the classical theory of solitons. Figures 13 and 16 show stable solitons in a toroidal plasma. Figures 11 and 12 show a bifurcation in a plasma torus. Figures 14 and 15 show the twisting and tearing of the plasma torus.

References

1. Kuznetsov, S. P. (2005). Example of a physical system with a hyperbolic attractor of the Smale-Williams type. Physical review letters, 95(14), 144101.
2. Kuznetsov, S. P. (2011). Dynamical chaos and uniformly hyperbolic attractors: from mathematics to physics. Physics-Uspekhi, 54(2), 119.
3. S.P.Kuznetsov. (2006). Chaotic dynamics in a physical system with a strange Smale – Williams attractor. JETP, 129(2), 400-412.
4. Arzhanukhina, D. S., & Kuznetsov, S. P. (2012). System of three non autono mous oscillators with hyperbolic chaos. Izv. vuzov. Prikladnaya nelineynaya dinamika, 20(6), 56.
5. Grebogi, C., Ott, E., Pelikan, S., & Yorke, J. A. (1984).

Strange attractors that are not chaotic. Physica D: Nonlinear Phenomena, 13(1-2), 261-268.
6. Hunt, B. R., & Ott, E. (2001). Fractal properties of robust strange nonchaotic attractors. Physical Review Letters, 87(25), 254101.
7. S.P.Kuznetsov. (2007). On the possibility of realization in the physical system of the strange non-chaotic attractor hunt and Ott. JTP, 77(4), 10-18.
8. Isaeva, O. B., Jalnine, A. Y., & Kuznetsov, S. P. (2006). Arnold's cat map dynamics in a system of coupled nonautonomous van der Pol oscillators. Physical Review E, 74(4), 046207.